Supplementary Information: Topological flat bands in a family of multilayer graphene moiré lattices

Dacen Waters[1,2*], Ruiheng Su[3,4*], Ellis Thompson[1*], Anna Okounkova[1], Esmeralda Arreguin-Martinez[5], Minhao He[1,6], Katherine Hinds[5], Kenji Watanabe[7], Takashi Taniguchi[8], Xiaodong Xu[1,5], Ya-Hui Zhang[9], Joshua Folk[3,4†], and Matthew Yankowitz[1,5†]

[1] *Department of Physics, University of Washington, Seattle, Washington, 98195, USA*

[2] *Intelligence Community Postdoctoral Research Fellowship Program, University of Washington, Seattle, Washington, 98195, USA*

[3] *Stewart Blusson Quantum Matter Institute, University of British Columbia, Vancouver, British Columbia, V6T 1Z1, Canada*

[4] *Department of Physics and Astronomy, University of British Columbia, Vancouver, British Columbia, V6T 1Z1, Canada*

[5] *Department of Materials Science and Engineering, University of Washington, Seattle, Washington, 98195, USA*

[6] *Department of Physics, Princeton University, Princeton, New Jersey, 08544, USA*

[7] *Research Center for Functional Materials, National Institute for Materials Science, 1-1 Namiki, Tsukuba 305-0044, Japan*

[8] *International Center for Materials Nanoarchitectonics, National Institute for Materials Science, 1-1 Namiki, Tsukuba 305-0044, Japan*

[9] *Department of Physics and Astronomy, Johns Hopkins University, Baltimore, Maryland, 21205, USA*

[*] *These authors contributed equally to this work. and*

[†] *jfolk@physics.ubc.ca (J.F.); myank@uw.edu (M.Y.)*

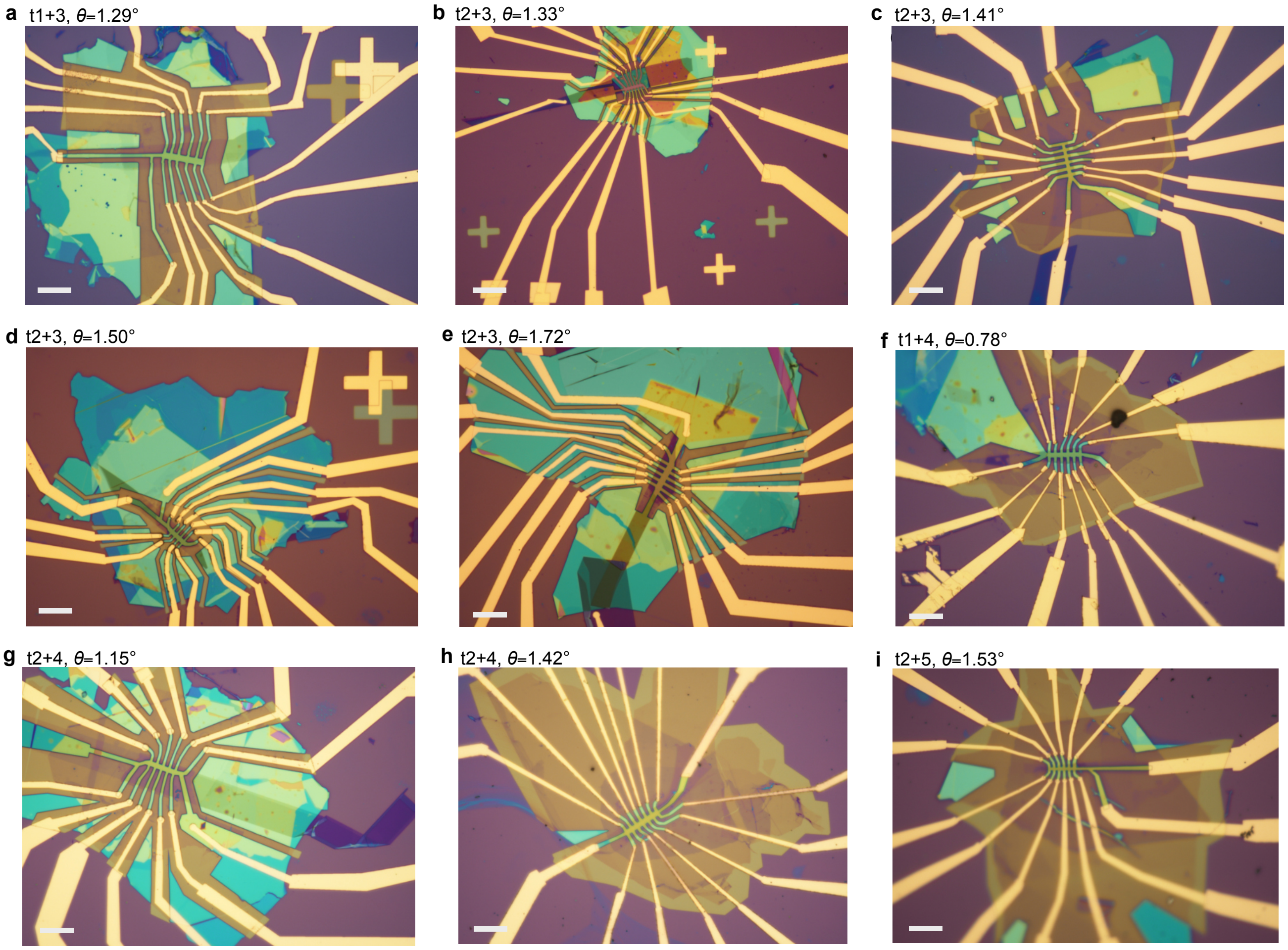

Supplementary Figure 1. **Optical micrographs of the t$M+N$ devices in this study. a-i,** All scale bars are 10 μm.

Supplementary Table 1: Summary of transport properties for all devices

tM+N	θ	D										
		$D \approx 0$	$D < 0$				$D > 0$					
		$\nu = 0$	$\nu = -4$	$\nu = 0$	$\nu = 2$	$\nu = 4$	$\nu = -4$	$\nu = 0$	$\nu = 1$	$\nu = 2$	$\nu = 3$	$\nu = 4$
t1+2	1.13°	-	BI	BI	CI†	BI	BI	BI	CI, AHE	CI	CI†	BI
t2+2	1.30°	-	BI	BI	CI	BI	BI	BI	CI†	CI	CI†	BI
t1+3	1.29°	-	BI	-	-	-	-	BI	CI†	CI	CI†, AHE	BI
t2+3	1.33°	I†	-	-	-	BI	BI	BI	-	-	-	BI
t2+3	1.41°	I	BI	BI	CI, $B > 0$	BI	BI	BI	CI, AHE	CI†	CI†	BI
t2+3	1.50°	I	BI	BI	CI†	BI	BI	BI	CI†, AHE	CI	CI†	BI
t2+3	1.72°	I		BI				BI				
t1+4	0.78°	-	BI	-	-	-	-	BI	-	-	-	BI
t2+4	1.15°	-	BI	-	-	-	-	BI	-	CI, $B > 0$	-	BI
t2+4	1.42°	I†	BI	-	-	-	-	BI	-	-	-	BI
t2+5	1.53°	I†	BI	-	-	-	-	BI	-	-	-	

- BI denotes a band insulator
- CI denotes a correlated insulator
- I denotes an insulator of unknown origin (i.e., cannot unambiguously distinguish between BI and CI)
- $B > 0$ indicates that the state is only observed in a magnetic field
- † indicates that transport features are suggestive of an incipient insulator, but not well developed at $B = 0$
- AHE denotes the presence of the anomalous Hall effect
- \- indicates a metallic state
- Empty cell indicates that our gate range does not include the specific state

ADDITIONAL TRANSPORT DATA

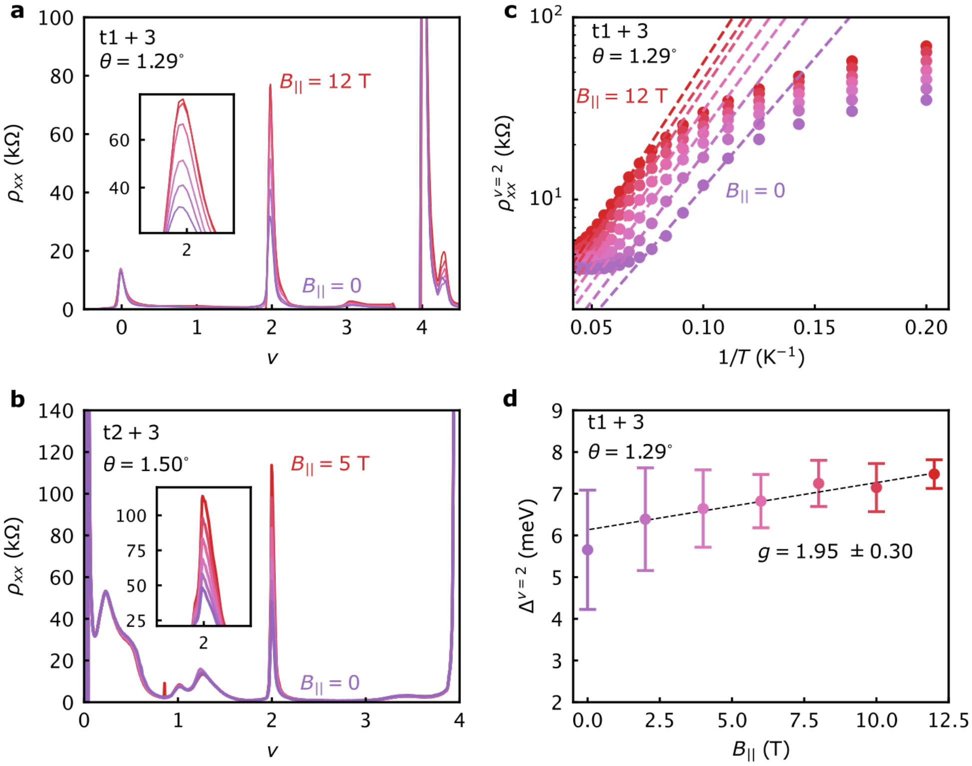

Supplementary Figure 2. **Evidence for spin-polarization at $\nu = 2$.** **a**, Measurement of ρ_{xx} versus ν for the t1 + 3 sample with $\theta = 1.29^\circ$ acquired at different values of $B_{||}$. The measurement is acquired at variable D in order to cut through the correlated states at each integer ν. The inset shows a zoom-in around $\nu = 2$, showing an increase in the resistance of the correlated insulator with $B_{||}$. The measurement was performed at $T = 1.7$ K. **b**, Similar measurement for the t2 + 3 device with $\theta = 1.50^\circ$, acquired at $D = 0.531$ V/nm and $T = 4$ K. **c**, ρ_{xx} acquired at $\nu = 2$ in the t1 + 3 device as a function of temperature, shown at different values of $B_{||}$ in increments of 2 T. The dashed lines show the linear fits in the thermally activated regime used to extract the gap size of the correlated insulator (see Methods). **d**, Extracted gap sizes determined by the fits shown in **c**. Error bars are standard deviations from the fits. The dashed black line shows the best linear fit to the experimentally determined gap sizes. The slope yields a g-factor consistent with $g = 2$ (see Methods), consistent with a spin-polarized insulator.

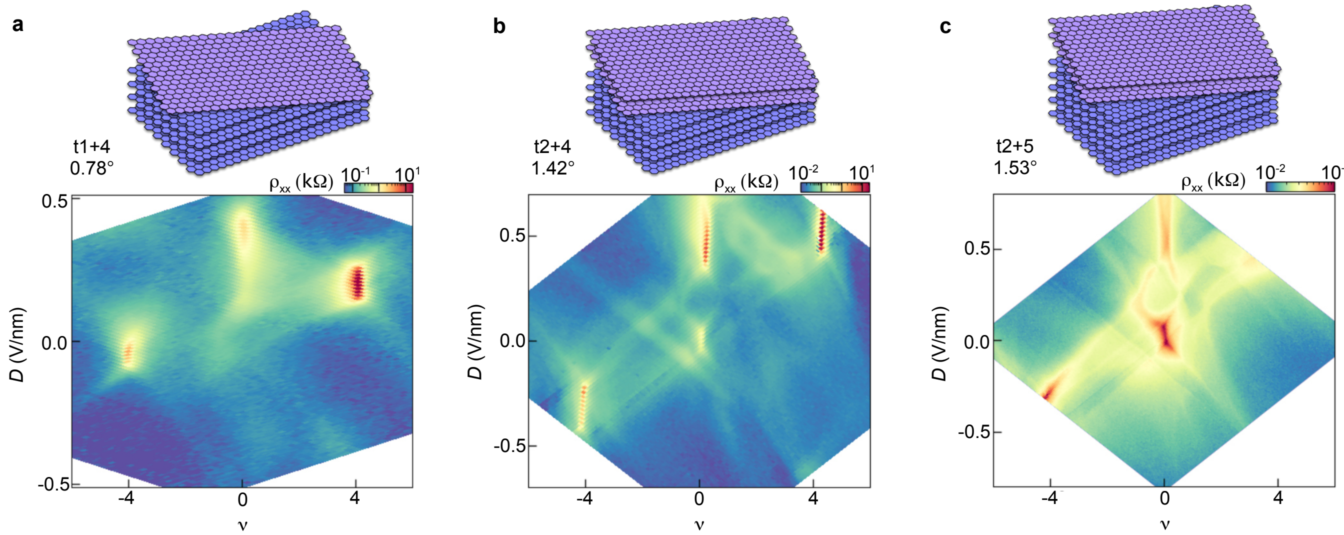

Supplementary Figure 3. **Additional t$M+N$ devices.** **a**, ρ_{xx} map of a t1 + 4 device with $\theta = 0.78^{\circ}$ acquired at $B = 0$ T. High-resistance states emerge over a small range of D at $\nu = 0$ and $\nu = \pm 4$, indicating the emergence of isolated moiré bands. **b**, Similar measurement for a t2+4 device with $\theta = 1.42^{\circ}$. **c**, Similar measurement for a t2+5 device with $\theta = 1.53^{\circ}$. Schematic above each map shows cartoon representations of the given twisted M- and N-layer combination. Measurements for **a-b** were acquired at $T = 1.5$ K. Measurements for **c** were acquired at $T = 100$ mK.

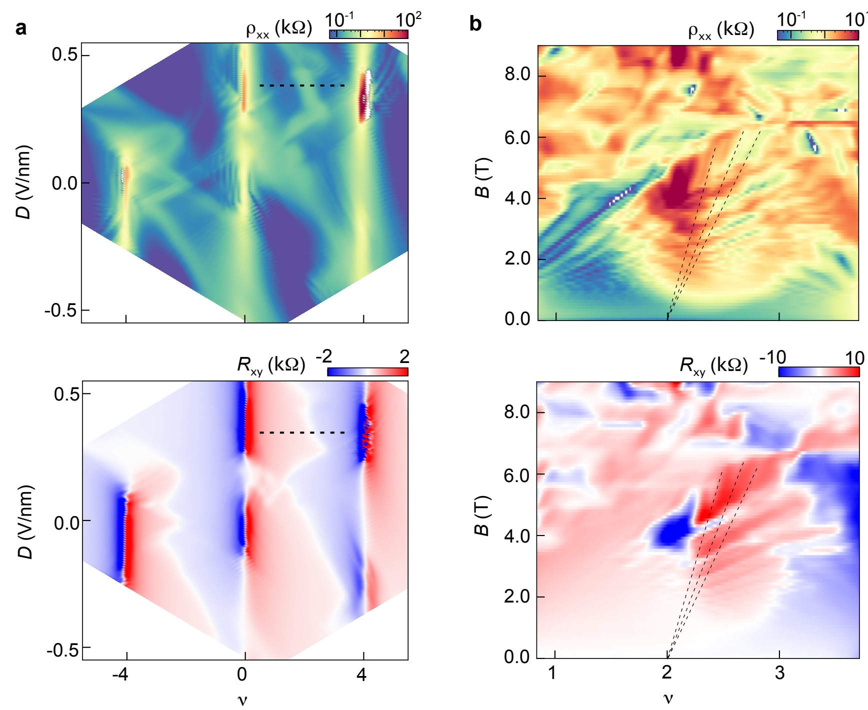

Supplementary Figure 4. **High-field correlated state in a t2 + 4 device.** **a**, ρ_{xx} (top) and R_{xy} (bottom) maps for the t2 + 4 device with $\theta = 1.15^{\circ}$ (the same as shown in Fig. 1h of the main text). The longitudinal (Hall) maps are symmetrized (anti-symmetrized) at $B = 0.5$ T. **b**, Landau fan diagrams acquired at $D = 0.35$ V/nm over the range of doping range indicated by dashed line in **a**. A high-resistance state accompanied by an abrupt sign reversal in R_{xy} emerges at $\nu = 2$ for $B \approx 4$ T. There are additionally quantum oscillations associated with this state that project to $\nu = 2$ at $B = 0$. Together, these observations indicate the emergence of a symmetry-broken state at $\nu = 2$ in a magnetic field. This state is destroyed at higher field by competition with other quantum Hall states. All measurements were acquired at $T = 100$ mK.

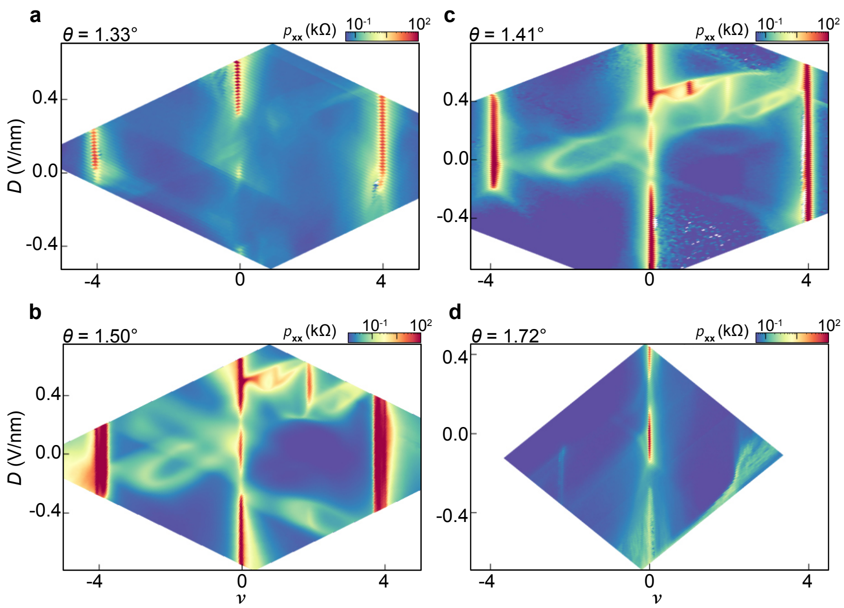

Supplementary Figure 5. **Twist angle dependence of t2+3.** ρ_{xx} map as a function of ν and D for four 2+3 devices with different twist angles: **a**, $\theta = 1.33°$ **b**, $1.41°$ **c**, $1.56°$, and **d** $1.72°$. Data shown in **a**, **b** and **c** feature insulating states at $\nu = 0$ and $\nu = \pm 4$. Only devices shown in **b** and **c** exhibit correlated insulating states at positive D for partial filling of the moiré conduction band. In addition, **c** further shows a correlated insulating state at negative D. All data taken at $T = 1.5$ K.

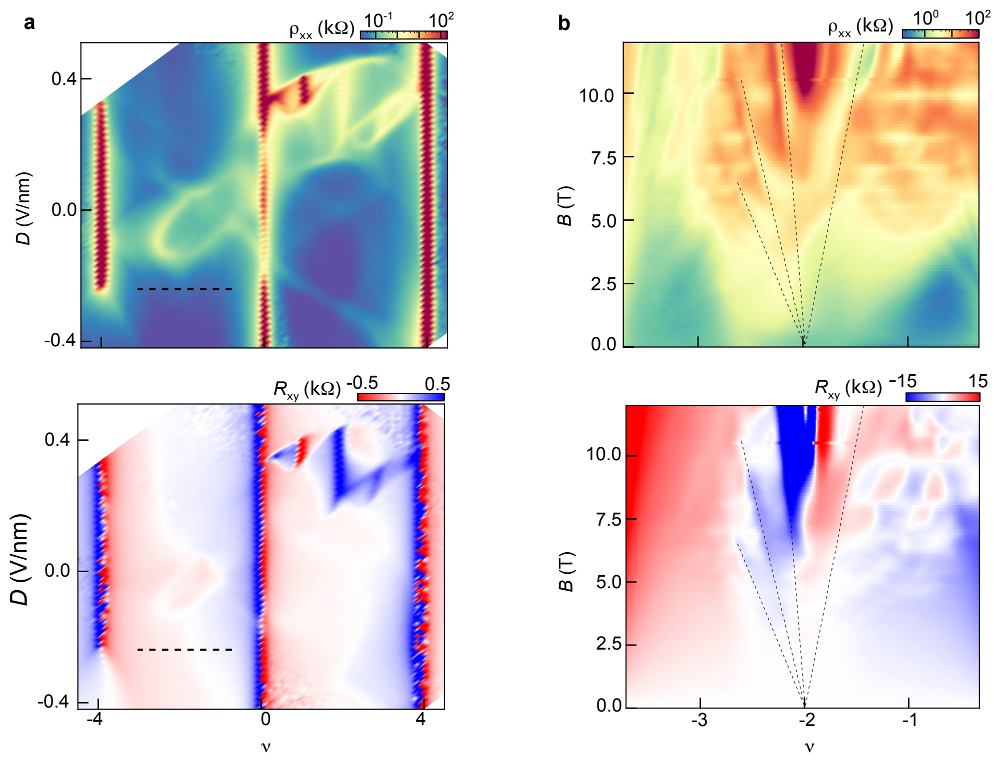

Supplementary Figure 6. **Correlated states at high field in a t2+3 device with $\boldsymbol{\theta = 1.41°}$.** **a**, ρ_{xx} (top) and R_{xy} (bottom) maps. The longitudinal (Hall) maps are symmetrized (anti-symmetrized) at $B = 0.1$ T **b**, Landau fans acquired at $D = -0.25$ V/nm over the doping range indicated by dashed line in **a**. The data shows clear quantum oscillations projecting to $\nu = -2$ at $B = 0$, associated with a high-resistance state accompanied by an abrupt sign reversal in R_{xy} above $B \approx 10$ T. Together, these observations indicate the emergence of a symmetry-broken state at $\nu = 2$ in a magnetic field. All measurements were acquired at $T = 1.5$ K.

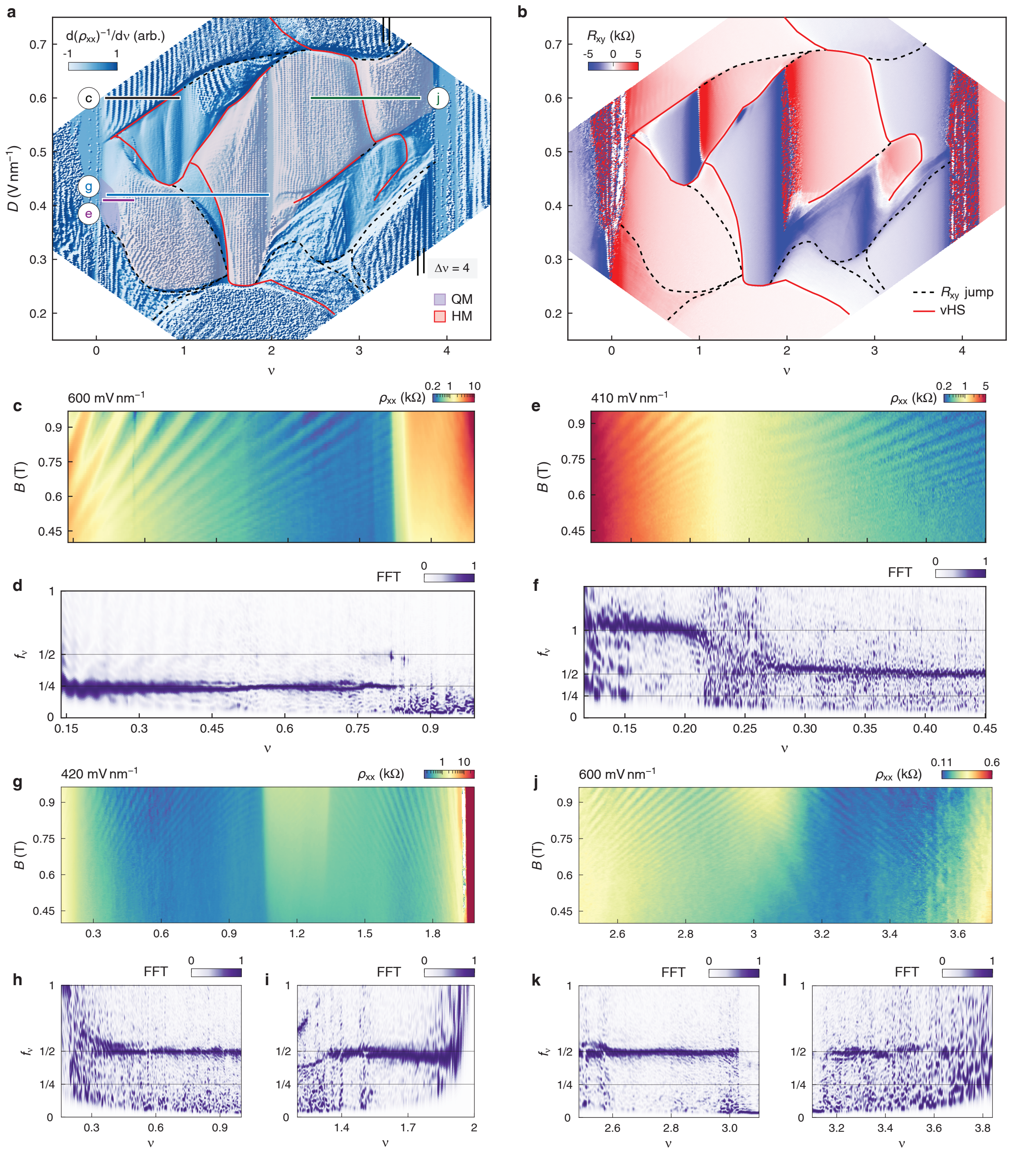

Supplementary Figure 7. **Analysis of phase boundaries and quantum oscillations in the t2+3 device with $\theta = 1.50°$.** **a**, Numerical derivative of $1/\rho_{xx}$ with respect to ν, highlighting the quantum oscillations (QOs) at $B = 0.9$ T. Red/purple shaded regions correspond to the half/quarter metal (HM/QM) regions in the phase diagram shown in Fig. 3a of the main text (only a subset of all symmetry-broken regions are shaded here for clarity). Labels c-j associated with lines of constant D show where data in the panels with the same label were obtained. **b**, Expanded view of the antisymmetrized R_{xy} obtained at $B = 0.9$ T overlaid with contours of $R_{xy} = 0$ (vHS) and R_{xy} jumps. **c** - **l**, Landau fan diagrams obtained at fixed D, and their corresponding FFT spectrum (where the FFT signal is normalized to the maximum value for each measurement). In **c**, The dominant frequency occur at $f_\nu = 1/4$, indicating that the area of a cyclotron orbit is 1/4 of the total Luttinger volume, corresponding to a normal metal with four-fold spin and valley degeneracy. The spectra at each ν have been normalized by the maximum amplitude at that band filling. For QOs that originate from an integer filling $\nu \neq 0$, the zero of ν was set to that band filling before performing the FFT analysis. In **i** and **k**, the zero was set to $\nu = 2$. In **l**, the zero was set to $\nu = 4$. For ease of comparison, the horizontal axes are shown as ν without any offsets. With the exception of **a**, **b**, which was obtained at $T = 100$ mK, the remaining panels were obtained at the base mixing chamber temperature of $T = 10$ mK.

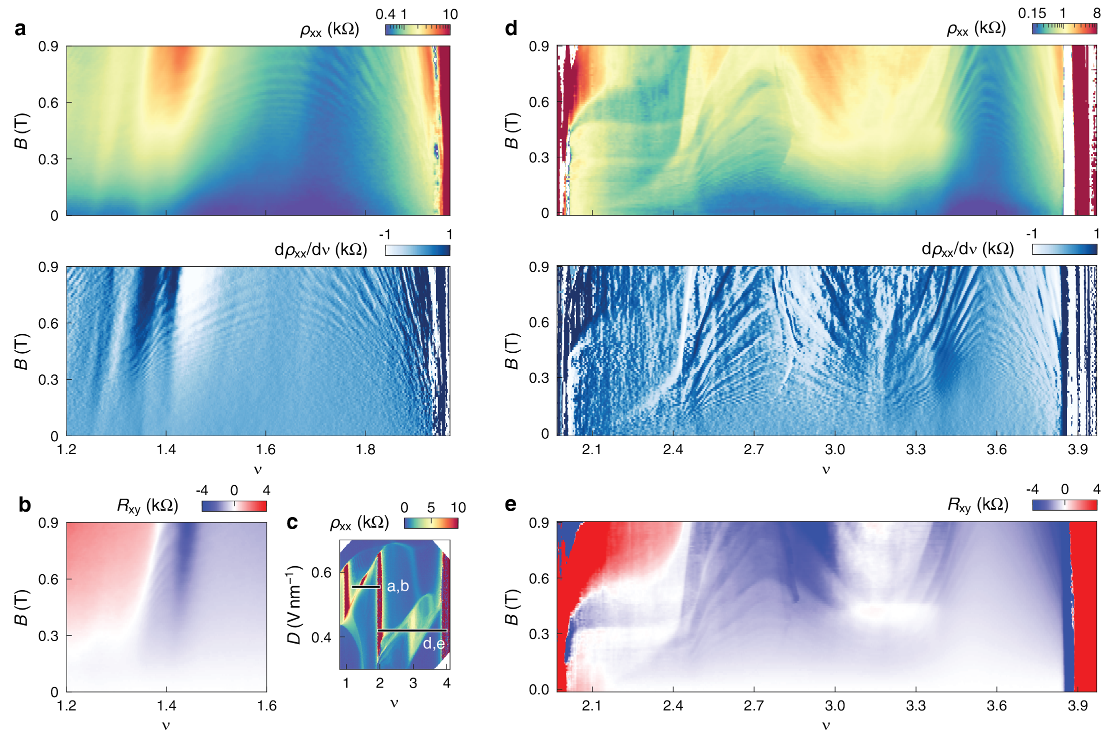

Supplementary Figure 8. **Signatures of multiband transport in the t2+3 device with $\theta = 1.50°$.** **a**, Longitudinal resistance and its numerical derivative obtained between $\nu = 1$ and 2, highlighting the evolution of curved quantum Hall states developing at low-B. **b**, Hall resistance as a function of B. **c**, Zoomed-in view of the phase diagram shown in the main text for reference. Horizontal lines indicate the displacement fields $D = 0.555$ V/nm and $D = 0.450$ V/nm where panels (**a**,**b**) and (**d**,**e**) were respectively obtained. **d**, **e**, Longitudinal and Hall resistance obtained near $\nu = 3$. Measurements were obtained at the base mixing chamber temperature of $T = 10$ mK.

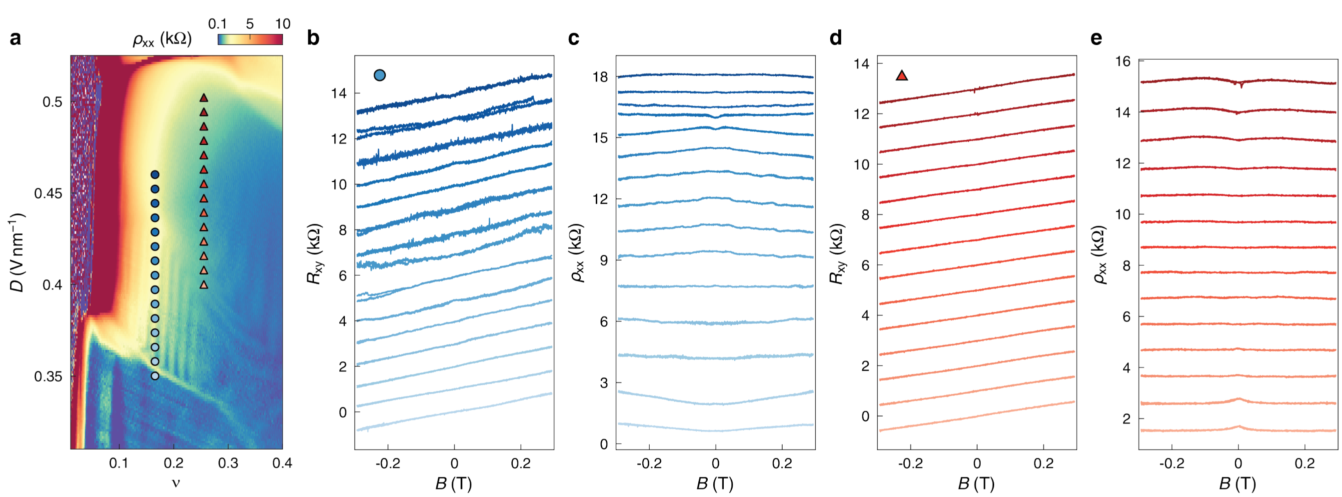

Supplementary Figure 9. **Hall and longitudinal magnetoresistance at low density in the t2+3 device with $\theta = 1.50°$.** **a**, High resolution ρ_{xx} map reproduced from Fig. 3b, focusing on regions that show no quantum oscillations (near $\nu = 0.25$, D between 0.45 and 0.5 V/nm) or fully degeneracy lifted quantum oscillations (near $\nu = 0.2$, D between 0.35 and 0.45 V/nm). **b**, **c**, ρ_{xy}, ρ_{xx} measured by sweeping B back and forth, obtained at fixed $\nu = 0.17$ (circle markers in **a**). Traces at different ν, D settings have been offset by 1 kΩ. **d**, **e**, Similar measurements to **b** and **c**, obtained at fixed $\nu = 0.26$ (triangle markers in **a**). Data at each location have been offset by 1kΩ for clarity. None of the measurements show evidence for the anomalous Hall effect, even in the quarter-metal region. Measurements were obtained at $T = 100$ mK.

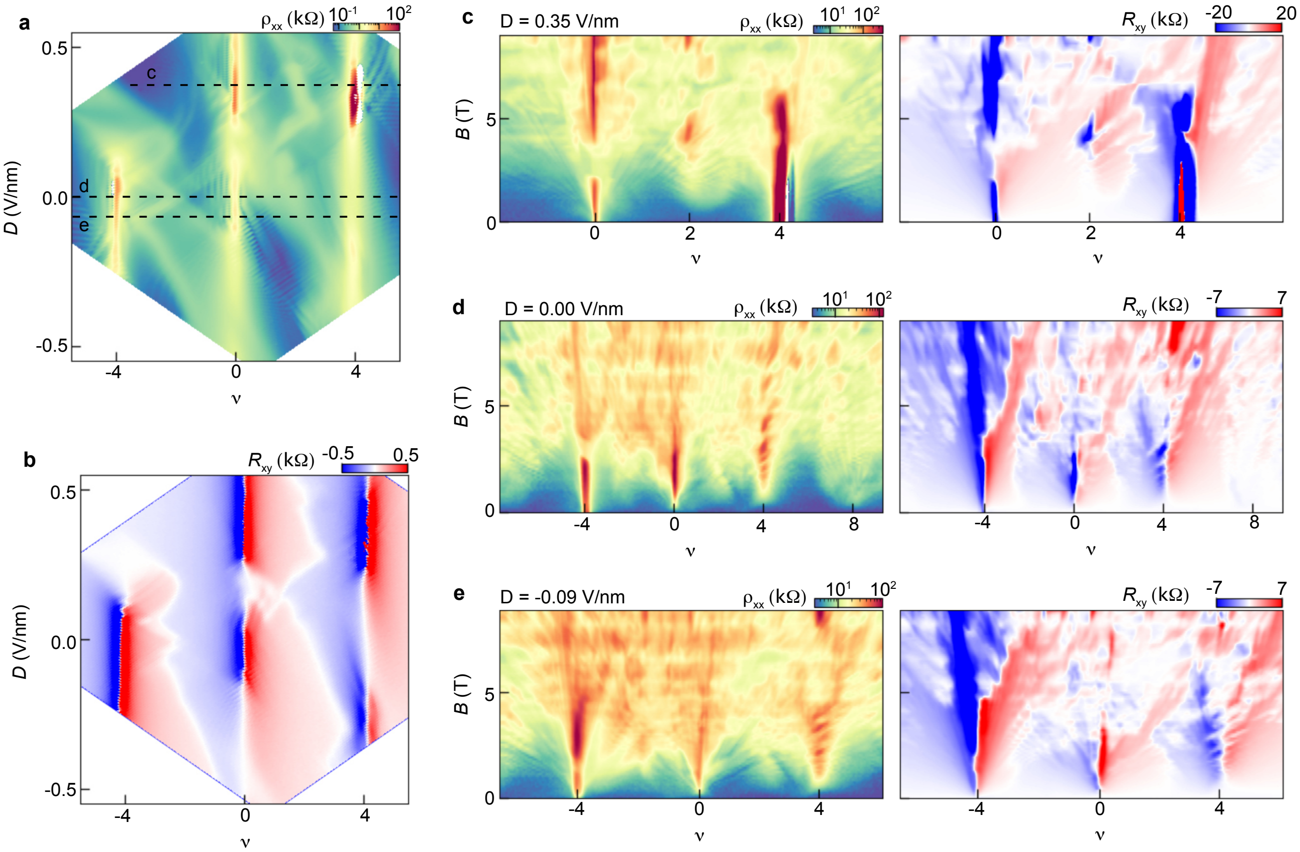

Supplementary Figure 10. **Additional Data for t2 + 4.** **a**, Longitudinal and **b,** Hall resistance maps in the t2+4 device $\theta = 1.42°$. The longitudinal (Hall) maps are symmetrized (anti-symmetrized) at $B = 0.5$ T. **c-e**, Landau fan diagrams acquired at fixed displacement fields of **(c)** $D = 0.35$ V/nm, **(d)** $D = 0$, and **(e)** $D = -0.09$ V/nm. All measurements in figure were acquired at $T = 100$ mK.

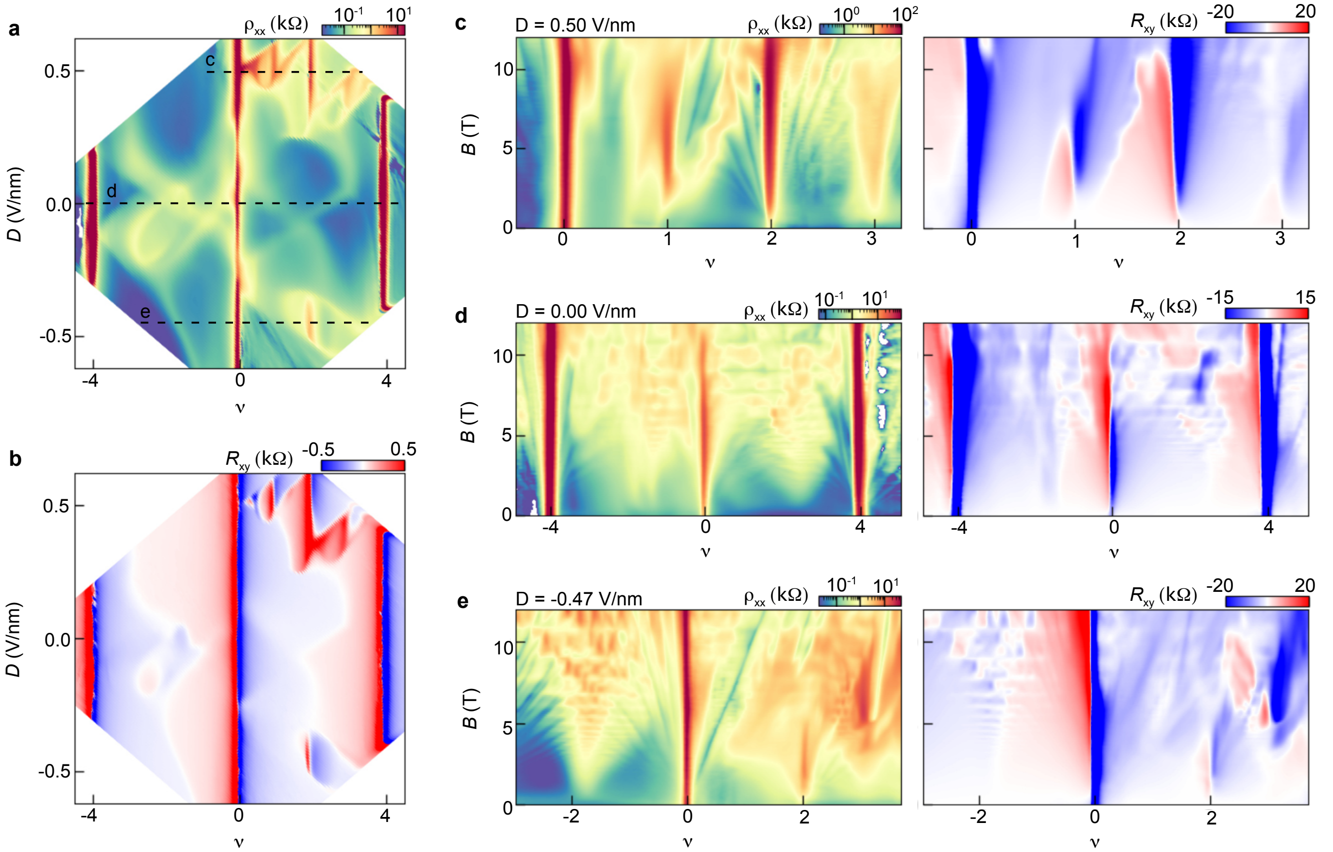

Supplementary Figure 11. **Additional Data for t2 + 3.** **a**, Longitudinal and **b,** Hall resistance maps in the t2+3 device with $\theta = 1.50^{\circ}$. The longitudinal (Hall) maps are symmetrized (anti-symmetrized) at $B = 0.1$ T. **c-e**, Landau fan diagrams acquired at fixed displacement fields of **(c)** $D = 0.50$ V/nm, **d** $D = 0$, and **e** $D = -0.47$ V/nm. All measurements in figure were acquired at $T = 1.5$ K.

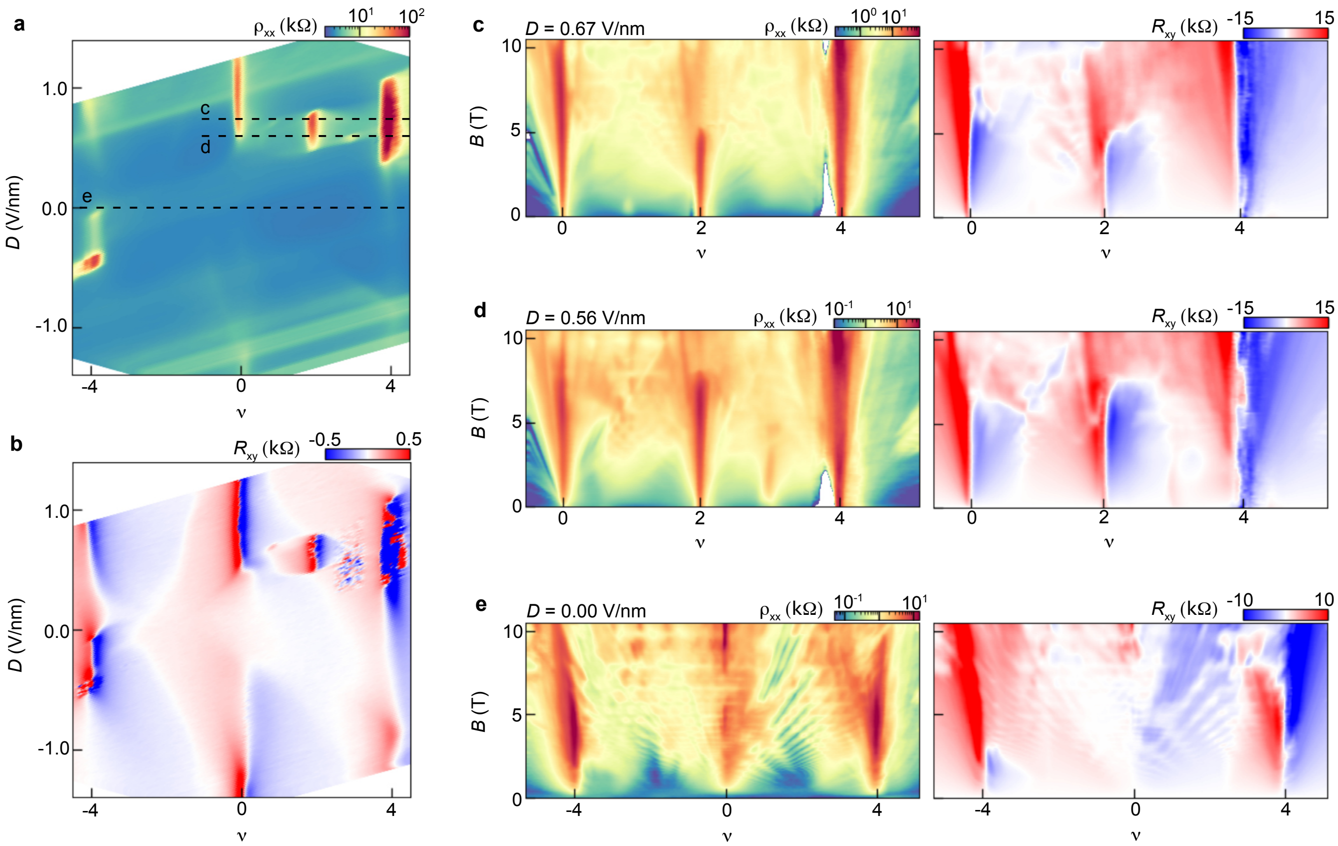

Supplementary Figure 12. **Additional Data for t1 + 3.** **a,** Longitudinal and **b,** Hall resistance maps in the t1+3 device. The longitudinal (Hall) maps are symmetrized (anti-symmetrized) at $B = 0.5$ T. **c-e,** Longitudinal and Hall resistances as a function of B at fixed displacement field of **c** $D = 0.67$ V/nm, **d** $D = 0.56$ V/nm, **e** $D = -0.00$ V/nm. All measurements in figure were acquired at $T = 1.5$ K.

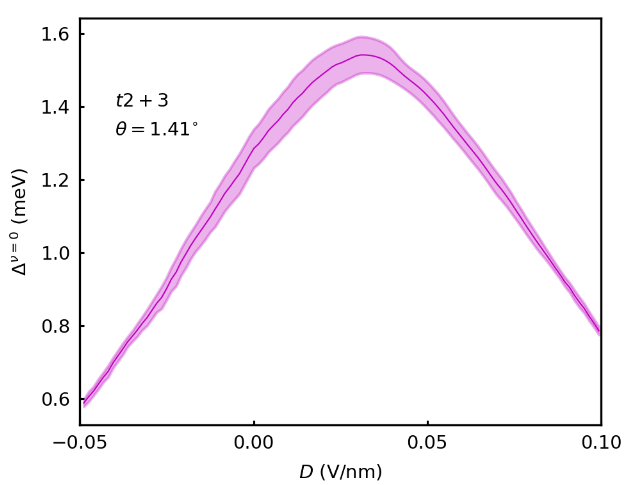

Supplementary Figure 13. **Measured gap size of the $\nu = 0$ insulating state in the t2 + 3 device with $\theta = 1.41^\circ$.** Gap size as a function of D at $\nu = 0$ (extracted from the data shown in Fig. 3e of the main text). The solid purple line denotes the best fit value from fitting Arrhenius plots, assuming $\rho_{xx} \propto \exp\left(\Delta^{\nu=0}/2k_BT\right)$. The shaded region denotes the standard deviation of the best fit value. The maximum value is found to be $\Delta^{\nu=0} = 1.54 \pm 0.05$ meV.

CONTINUUM MODEL CALCULATIONS

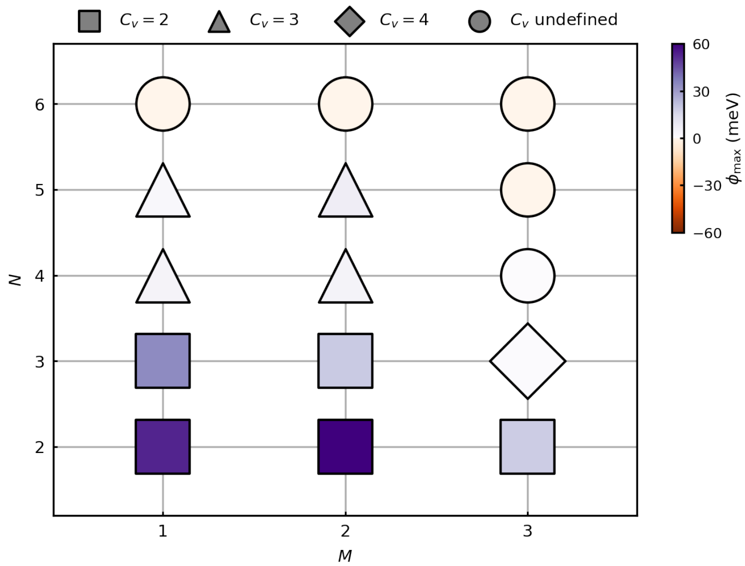

Supplementary Figure 14. **Calculated band isolation, flatness, and topology of various t$M+N$ structures.** Summary of the band structure calculations for all t$M+N$ combinations up to t$3+6$. The color of each marker indicates the maximum value of ϕ obtained after searching over all combinations of θ and δ. The valley Chern number of the moiré conduction band for each layer combination is also calculated for the optimal parameters of θ and δ, i.e., where $\phi = \phi_{\max}$. The shape of the markers indicates the valley Chern number. We do not calculate the valley Chern number for systems where the moiré conduction band cannot be isolated ($\phi_{\max} \leq 0$), indicated by the circle markers.

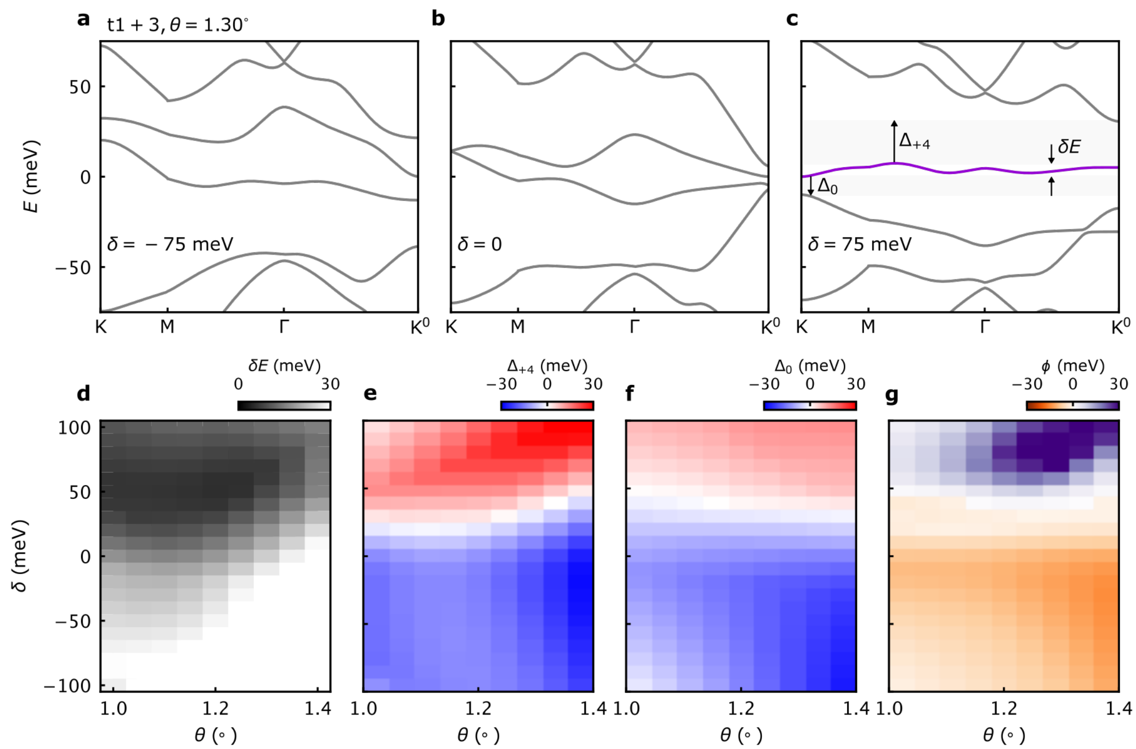

Supplementary Figure 15. **Band structure calculations for t1 + 3. a-c**, Band structures for the t1+3 system at 1.30°, with interlayer potentials $\delta = -75, 0$, and 75 meV, respectively. Panel **c** shows the definitions of Δ_0, Δ_{+4}, and δE. **d**, Bandwidth, δE, of the moiré conduction band calculated as a function of θ and δ. **e**, Energy separation between the top of the moiré conduction band and the top of the remote conduction band, Δ_{+4}. Positive (negative) values of Δ_{+4} indicate a band gap (band overlap). **f**, Similar plot, but for the energy separation between the moiré conduction and valence band, Δ_0 (i.e., the gap at the charge neutrality point). **g**, The isolated flat band parameter, ϕ (see Methods), as a function of twist angle and interlayer potential. Large positive values of ϕ (purple), corresponds to a flat and isolated moiré conduction band. Negative values of ϕ (orange) correspond to the moiré conduction band overlapping with other bands. The optimal twist angle is around 1.30°, corresponding to the band structures shown in panels **a-c**.

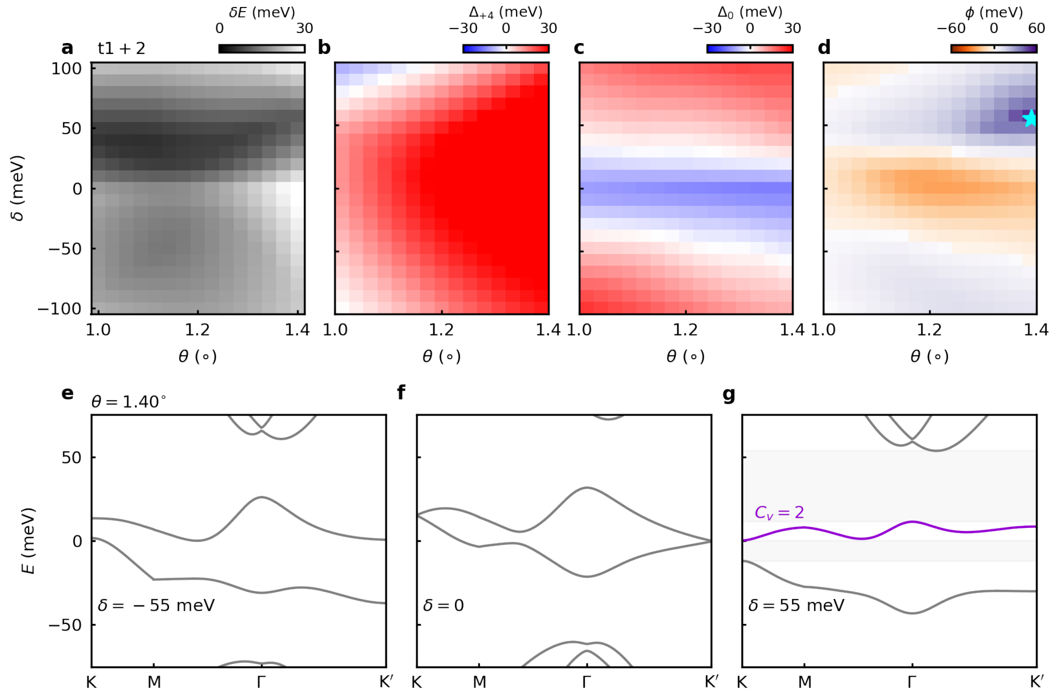

Supplementary Figure 16. **Single particle calculations for t1 + 2.** **a**, Bandwidth of the moiré conduction band, δE as a function of twist angle, θ, and interlayer potential, δ. **b**, Energy difference between the top of the moiré conduction band and the remote conduction band, Δ_{+4}. Positive values indicate a gap, negative values indicate band overlap. **c**, Energy difference between the bottom of the moiré conduction band and the top of the moiré valence band, Δ_0. **d**, Isolated flat band parameter, ϕ, see Methods for definition. Larger positive values indicates more flat and isolated moiré conduction band. Cyan star denotes the optimal parameter condition for a flat and isolated moiré conduction band. **e**-**g**, Representative band structures at the optimal angle condition at the indicated values of δ. In panel **g**, the moiré conduction band is highlighted in purple and shaded regions indicate gaps, i.e. it is isolated from other bands. The calculated valley Chern number, C_v, is shown for the flat and isolated moiré conduction band.

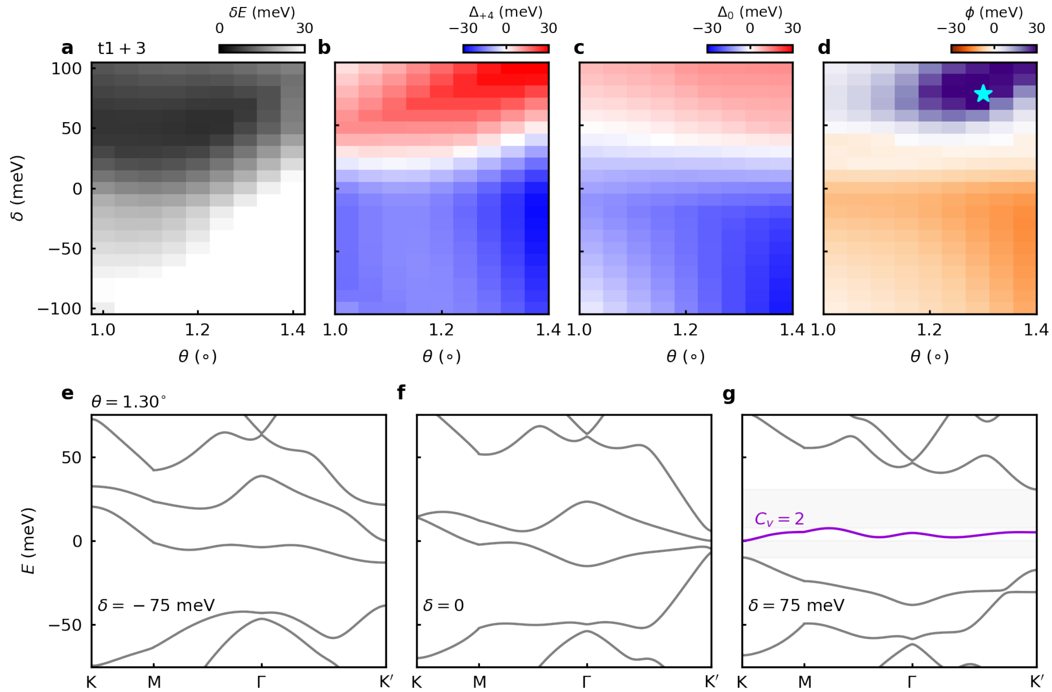

Supplementary Figure 17. **Single particle calculations for t1 + 3.** Similar to Supplementary Fig. 16.

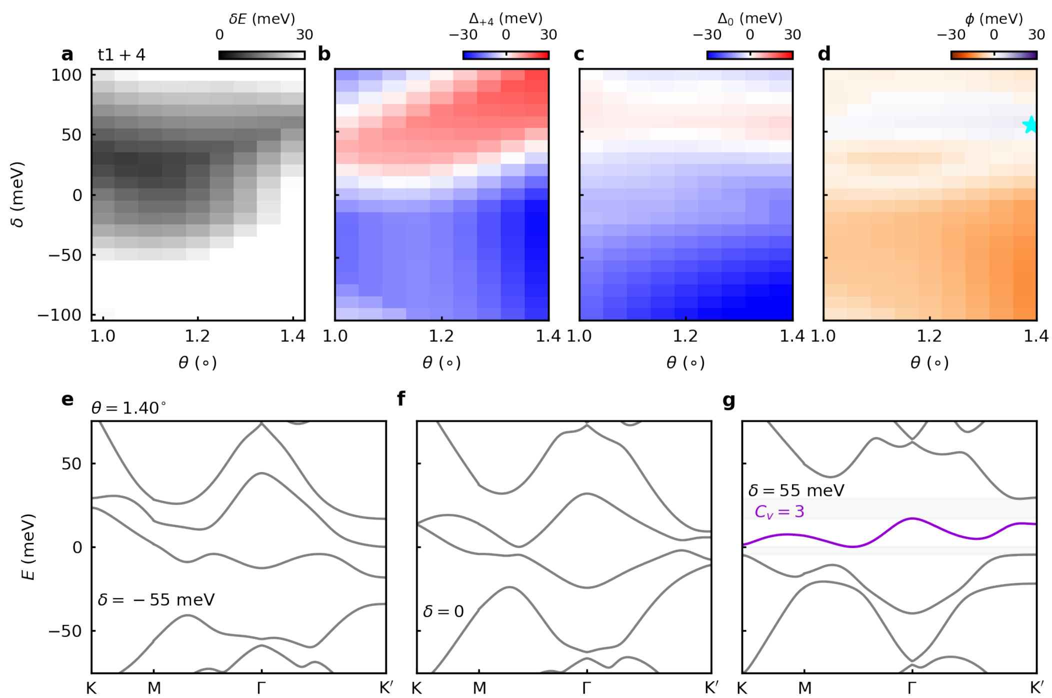

Supplementary Figure 18. **Single particle calculations for t1 + 4.** Similar to Supplementary Fig. 16.

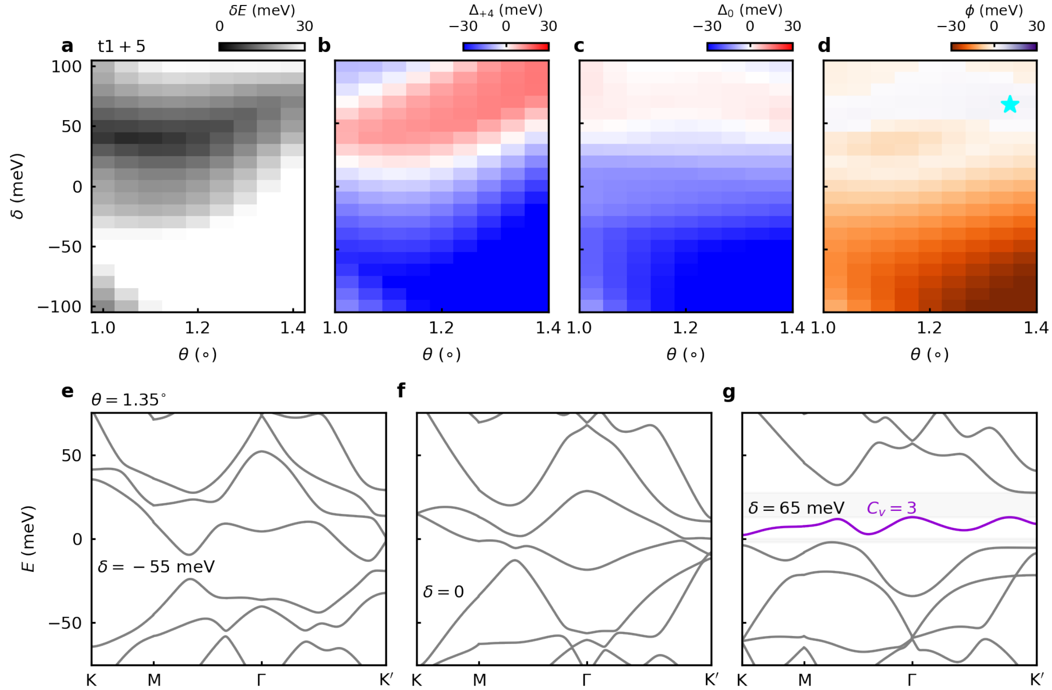

Supplementary Figure 19. **Single particle calculations for t1 + 5.** Similar to Supplementary Fig. 16.

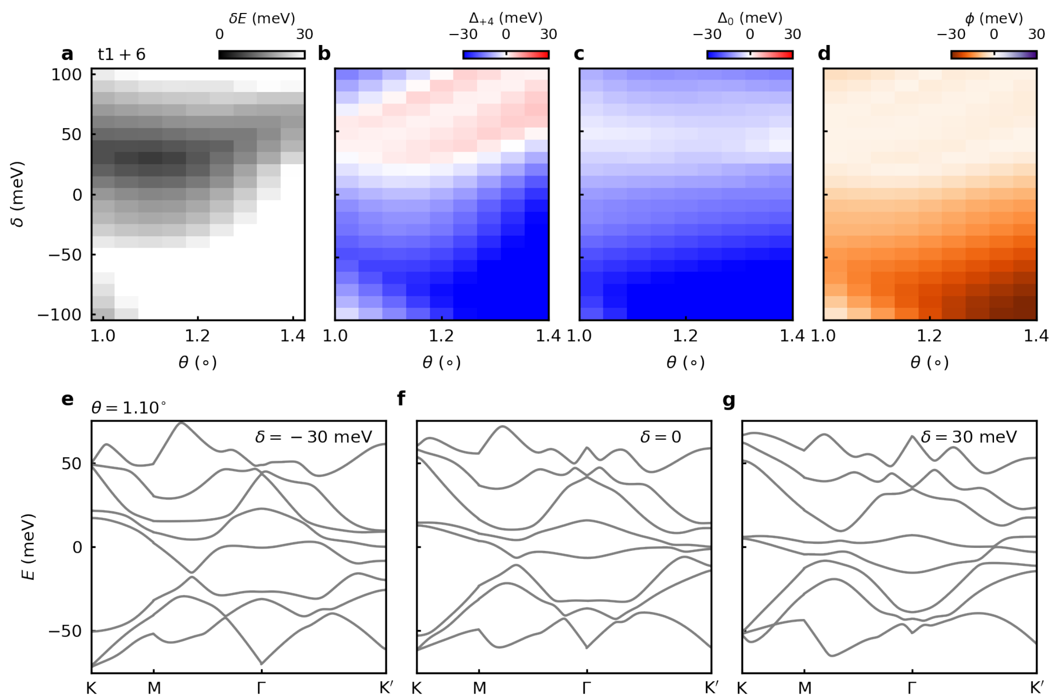

Supplementary Figure 20. **Single particle calculations for t1 + 6.** Similar to Supplementary Fig. 16. The moiré conduction band never becomes isolated for t1 + 6.

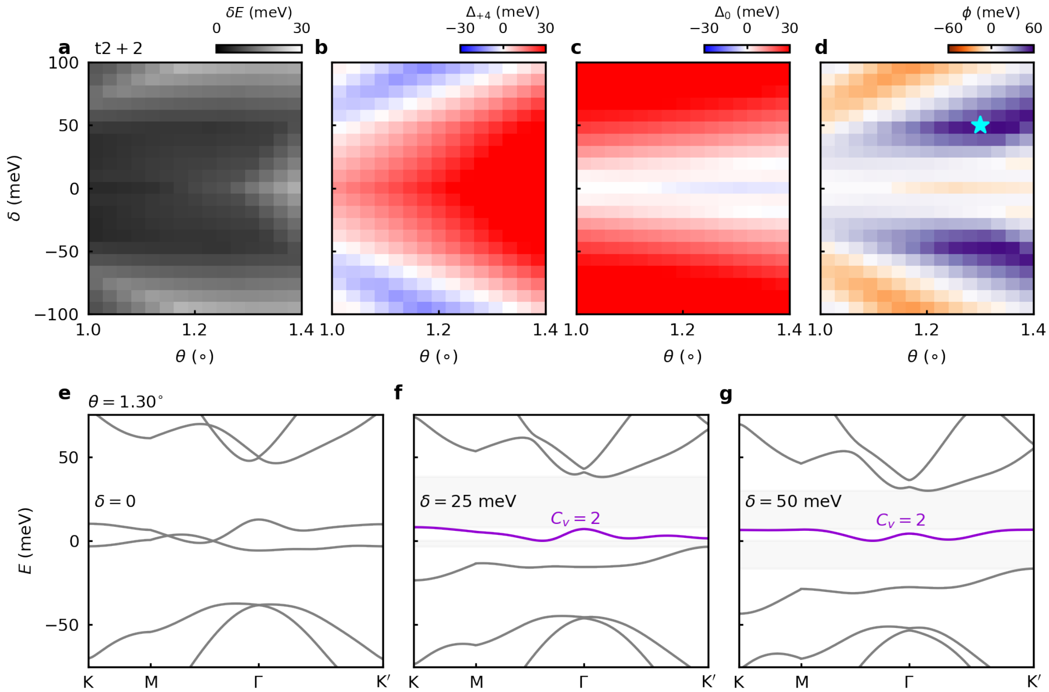

Supplementary Figure 21. **Single particle calculations for $\mathbf{t2+2}$.** Similar to Supplementary Fig. 16.

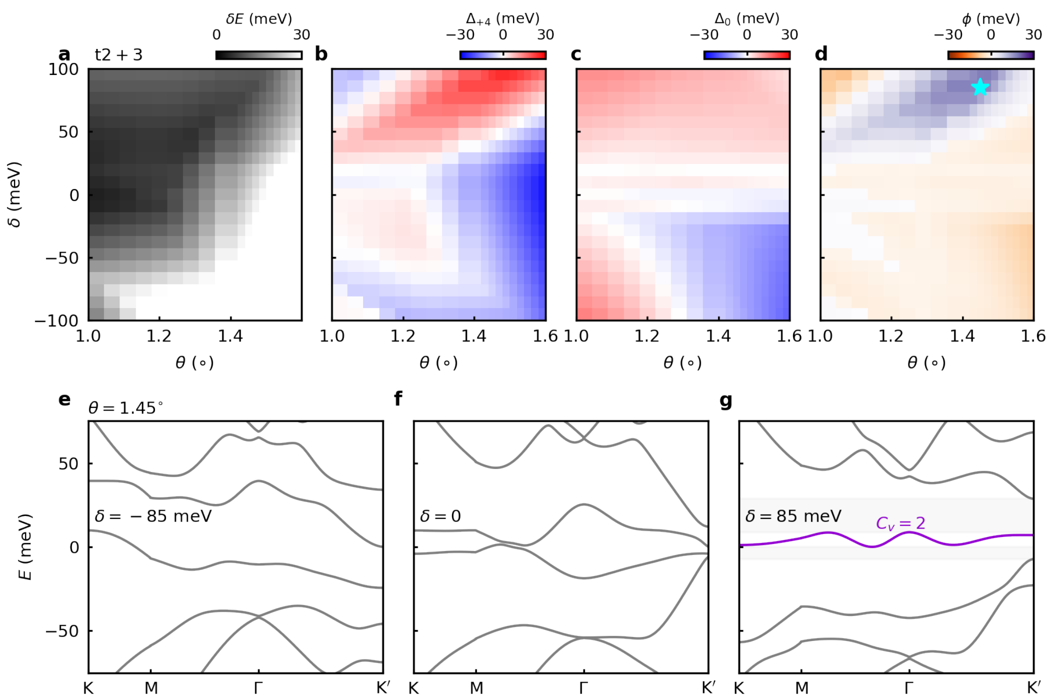

Supplementary Figure 22. **Single particle calculations for $\mathbf{t2+3}$.** Similar to Supplementary Fig. 16.

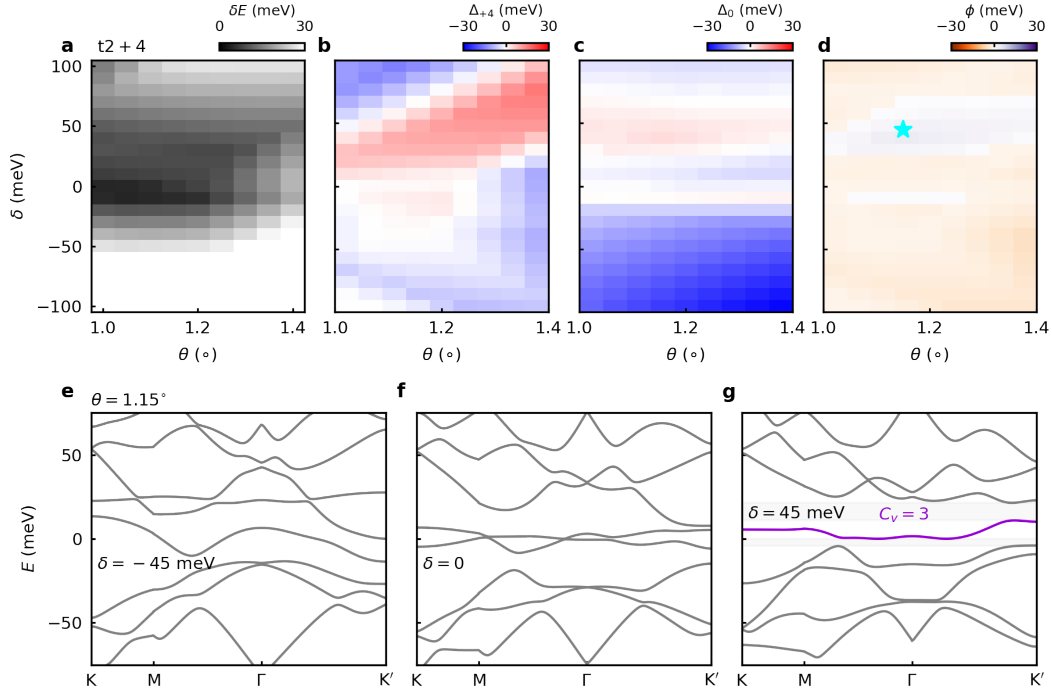

Supplementary Figure 23. **Single particle calculations for t2 + 4.** Similar to Supplementary Fig. 16.

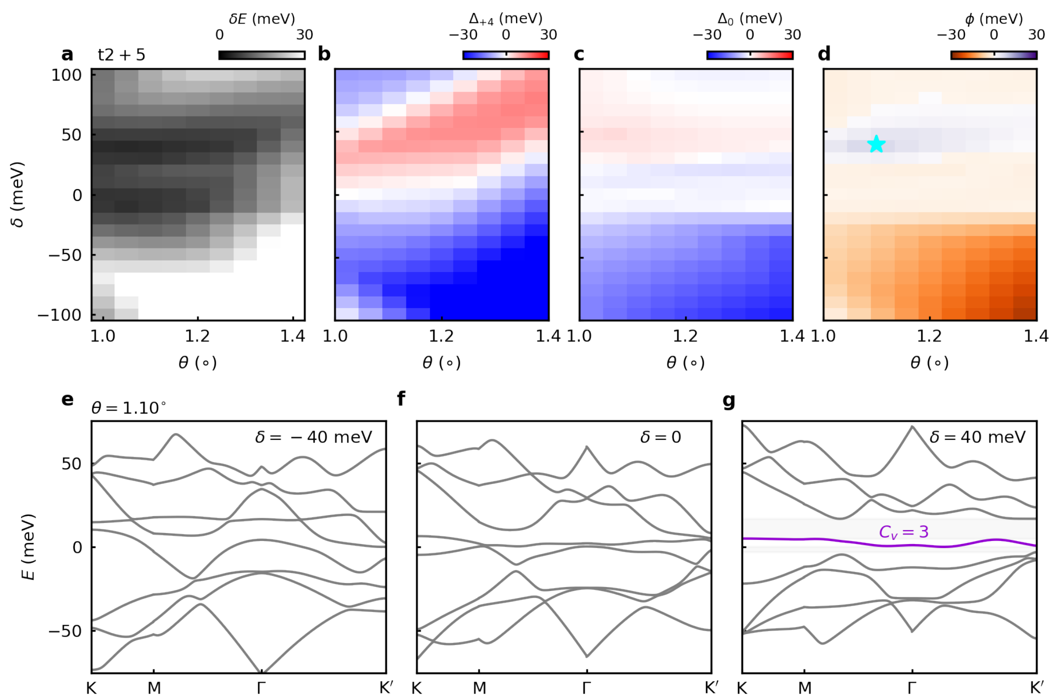

Supplementary Figure 24. **Single particle calculations for t2 + 5.** Similar to Supplementary Fig. 16.

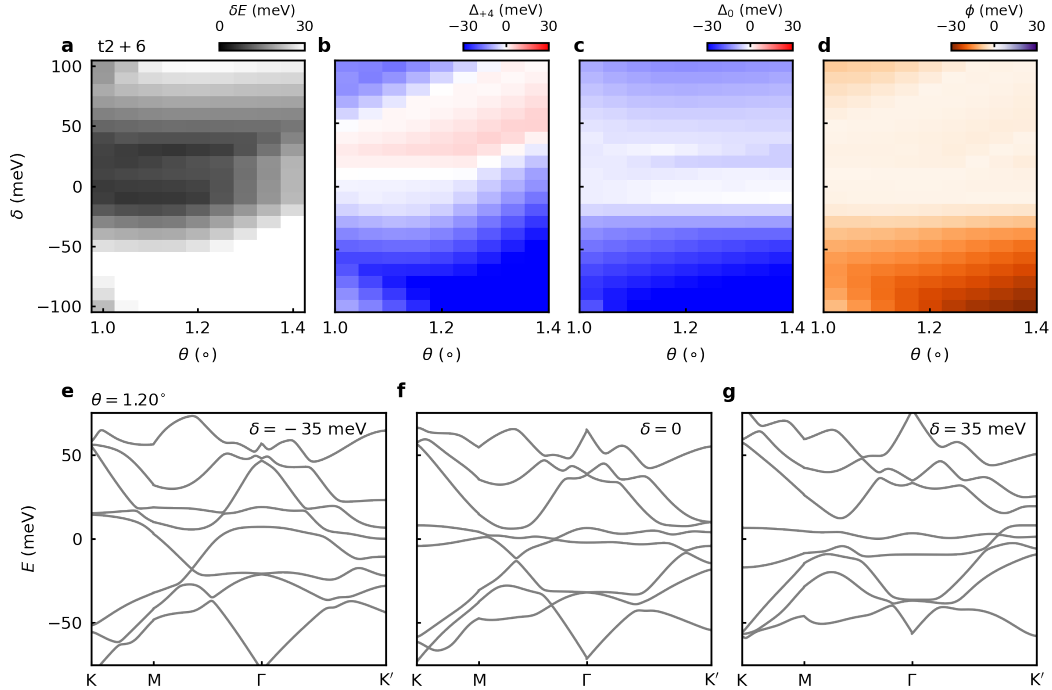

Supplementary Figure 25. **Single particle calculations for t2 + 6.** Similar to Supplementary Fig. 16. The moiré conduction band never becomes isolated for t2 + 6.

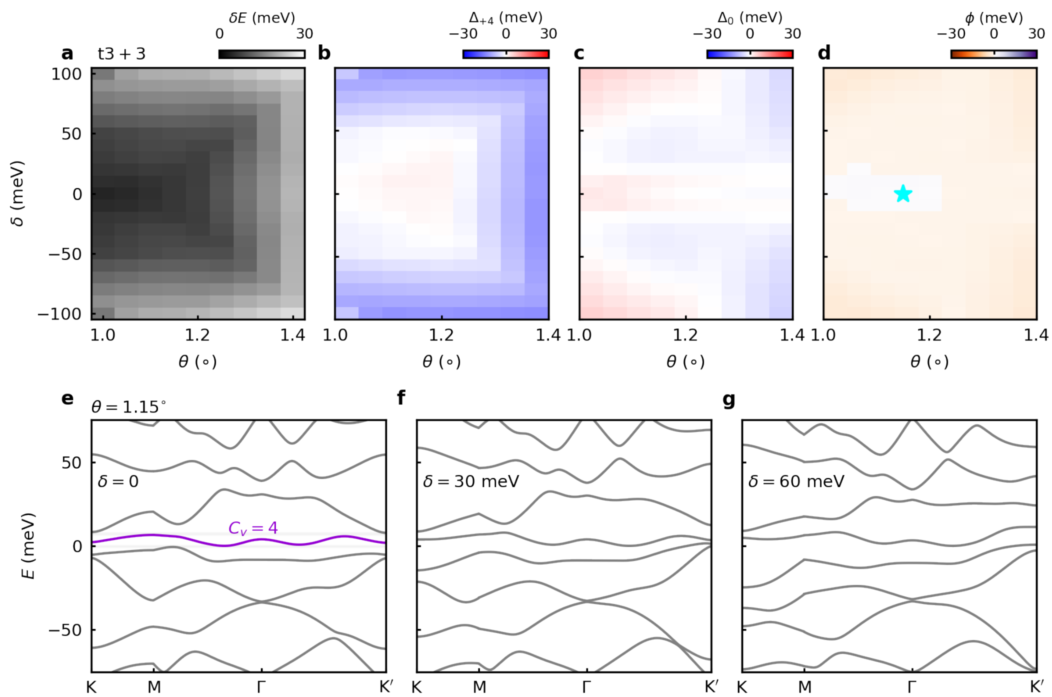

Supplementary Figure 26. **Single particle calculations for t3 + 3.** Similar to Supplementary Fig. 16.

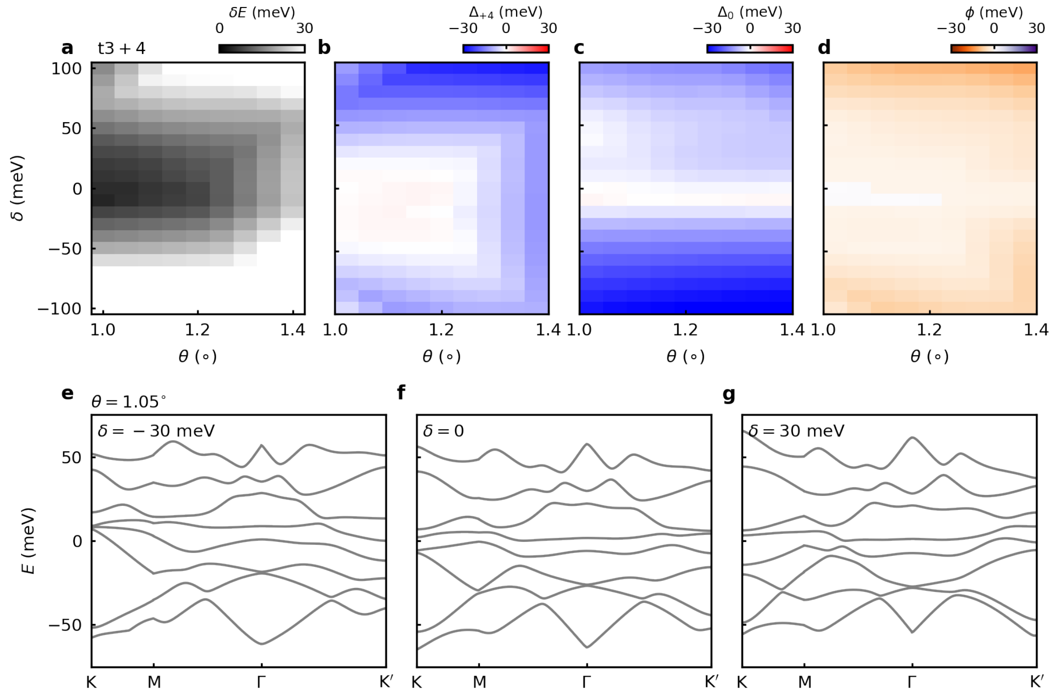

Supplementary Figure 27. **Single particle calculations for t3 + 4.** Similar to Supplementary Fig. 16. The moiré conduction band never becomes isolated for t3 + 4.

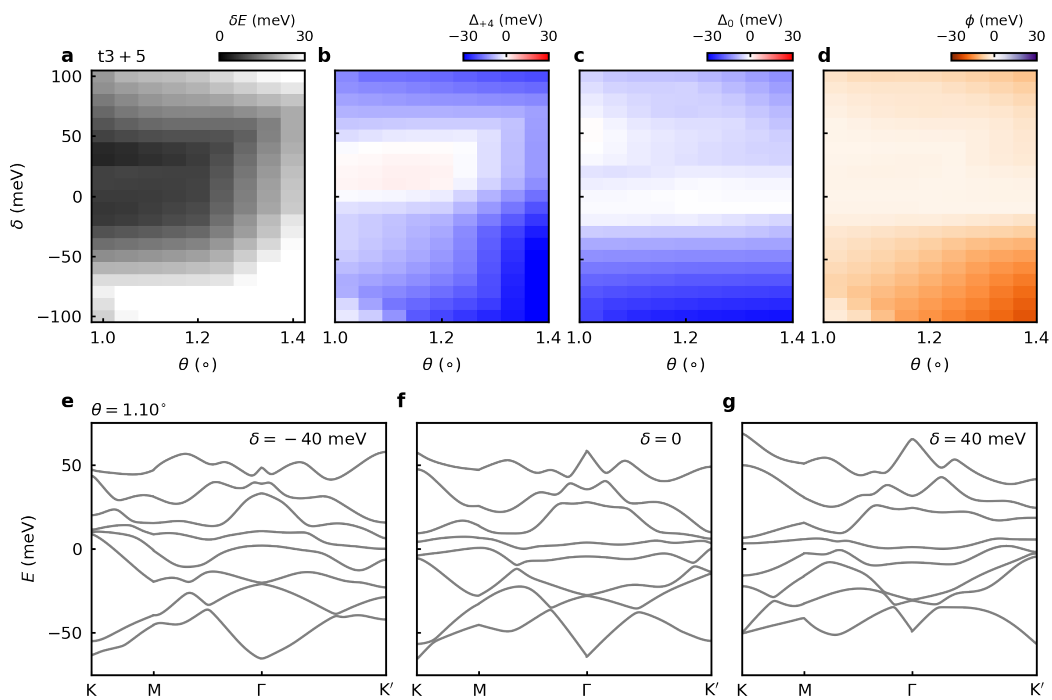

Supplementary Figure 28. **Single particle calculations for t3 + 5.** Similar to Supplementary Fig. 16. The moiré conduction band never becomes isolated for t3 + 5.

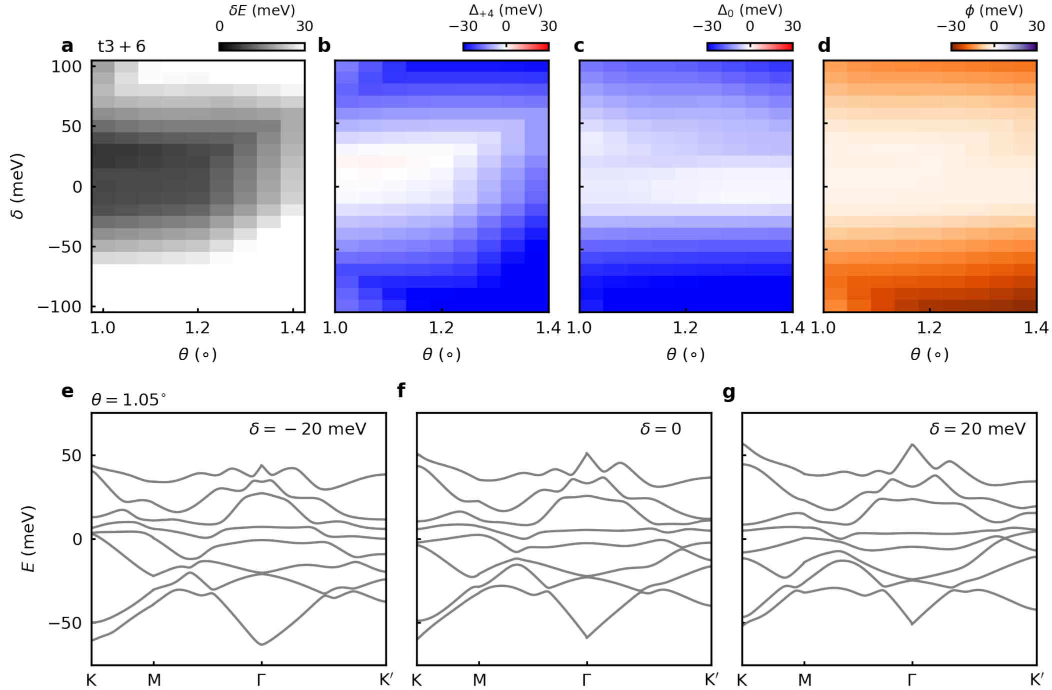

Supplementary Figure 29. **Single particle calculations for t3 + 6.** Similar to Supplementary Fig. 16. The moiré conduction band never becomes isolated for t3 + 6.

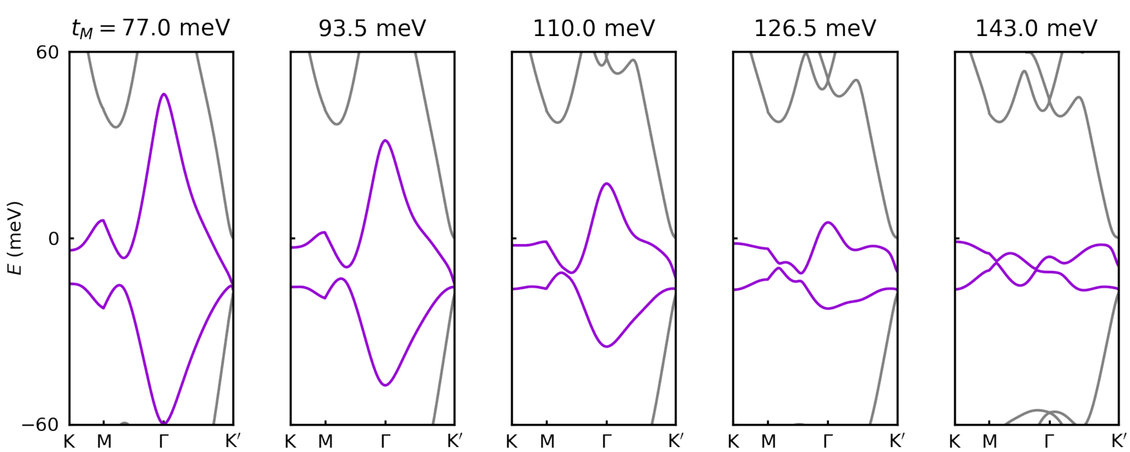

Supplementary Figure 30. **Band structure calculations for the $\theta = 1.50^{\circ}$ t2 + 3 at $\delta = 0$.** Calculation results shown for varying values of the moiré coupling parameter t_M. The nominal value we used for all other calculations is $t_M = 110$ meV (center panel). Here both the moiré conduction and moiré valence band are shown in purple, to emphasize that the bands always overlap, inconsistent with our observation of an insulating state in Fig. 3d & e of the main text.